UAV MULTISPECTRAL TIME-SERIES AND WEATHER-BASED HURDLE MODELING FOR ONION DISEASES AND PEST ESTIMATION

Ajay Pathak[1], Dimple Bhuta[2], Sagar Wayal[3], Rohit Kushwaha[2], Sanket Bhegde[2], Ashwini G.[2], Suresh Gawande[3]
[1]*Center for Machine Intelligence & Data Science, IIT Bombay, Mumbai, India*
[2]*TIH Foundation for IoT & IoE, IIT Bombay, Mumbai, India*
[3]*ICAR–Directorate of Onion & Garlic Research (DOGR), Rajgurunagar, Pune, India*

***Abstract*—Onion crops are highly vulnerable to a range of diseases and pests, which can lead to significant yield losses if timely detection and intervention are not achieved. This study presents a multimodal framework that integrates spectral indices derived from UAV-based multispectral imagery with meteorological data to estimate the incidence of major onion stressors under controlled field conditions. Data were collected from experimental plots of the Bhima onion variety across multiple growth stages, where stemphylium blight, anthracnose, purple blotch, and thrips co-occurred at naturally varying intensities. Fourteen vegetation indices (VI) and four weather variables were evaluated under untreated (no-spray) conditions to determine which features most reliably predict crop health and stress intensity. Beyond conventional indices, we incorporated derived features capturing temporal changes, lag effects, and biomass normalization, which significantly enhanced sensitivity to stress dynamics. Among all evaluated features, a newly introduced vegetation index, referred to as the Green Stress Ratio, consistently demonstrated the strongest associations across all disease and pest categories. A two-stage classification–regression framework was employed to first detect the presence of a stressor and subsequently quantify its severity, with models evaluated independently for each disease and pest. The results highlight the effectiveness of combining UAV-derived multispectral data with weather information for non-invasive, field-scale monitoring of onion crop health. This integrated approach provides a foundation for advanced decision-support systems aimed at targeted and sustainable pest and disease management in onion cultivation.**

***Index Terms*—Multispectral image analysis, vegetation indices–weather data fusion, time-series crop stress analysis, classification–regression framework, onion crop health monitoring**

I. Introduction

Onion (Allium cepa L.) is among the most extensively cultivated and consumed vegetable crops worldwide, owing to its broad culinary use, nutritional value, and comparatively long storage life. India remains the leading global producer of onions, with an estimated production of 24.21 million tonnes during 2023–2024 [1]. Onion crops are highly vulnerable to a combination of biotic and abiotic stresses. Major biotic stresses include diseases such as stemphylium blight, anthracnose, and purple blotch, as well as pests such as thrips, while abiotic stress stems from erratic rainfall, high humidity, and temperature fluctuations. Severe infestations can reduce bulb yields by 30–50%, posing a significant threat to total production [2]. Non-invasive disease and pest assessment using remote sensing and weather data offers a scalable, timely alternative to field scouting for objective crop health evaluation. UAV-based multispectral sensing enables high-resolution, farm-scale monitoring with reduced cloud sensitivity and reliable feature discrimination [3]. Building on this, the study integrates UAV multispectral imagery with weather data to estimate disease and pest incidence in 'Bhima' onions (Fig. 1). Field trials were conducted at the Directorate of Onion and Garlic Research (DOGR), Maharashtra, India.

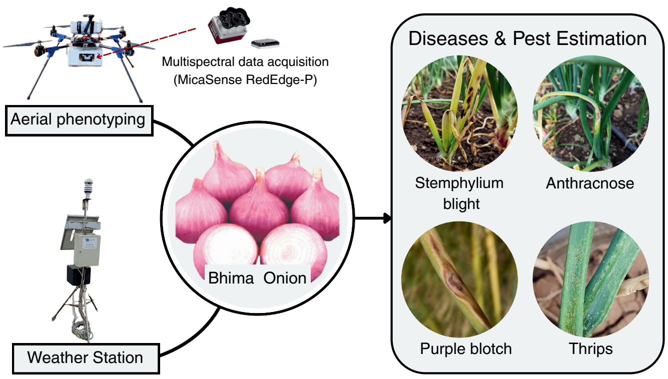

Fig. 1. Overview of the disease and pest estimation framework using multispectral UAV imagery and ground-based weather data for Bhima onion.

Multispectral frameworks for onion health monitoring have shown promise, though challenges remain. For instance, [4] reported over 85% accuracy in anthracnose–twister detection using multispectral UAV imagery with object-based image analysis and an SVM classifier. In contrast, [5] reported weak correlations between standard vegetation indices and stemphylium leaf blight severity, underscoring the limitations of conventional spectral features for certain diseases. These findings highlight the need to incorporate weather data, a key driver of pest and disease dynamics. Relative humidity and temperature strongly influence thrips populations [6], while temperature, humidity, and rainfall govern purple blotch progression [7]. Similar multi-source approaches have improved prediction and mapping of wheat stripe rust by integrating spectral and weather data [8, 9]. By fusing high-resolution UAV multispectral and weather data, this study addresses the limitations of single-source sensing for robust onion health assessment. The following sections describe field experiments at DOGR, multimodal data acquisition, and the machine learning pipeline, followed by performance evaluation and application for automated monitoring.

II. Methodology

A. Experimental Site and Field Protocols

Field trials were conducted at DOGR using the 'Bhima Super' red onion variety, with the experimental layout illustrated in Fig. 2. A total of 11 field trials were conducted from 28 August 2023 to 28 March 2024, covering key onion growth stages including the vegetative stage, bulb initiation stage, and bulb development stage. The trials followed a rectangular block design with five treatments and three replications per treatment; however, this study exclusively focuses on the untreated control plots to capture the natural, co-occurring progression of diseases and pest. To ensure temporal consistency, UAV and weather data were collected on the same day, while ground truth observations were recorded within one week of flights. Disease severity was quantified using Percent Disease Index (PDI) for stemphylium blight, anthracnose, and purple blotch, while thrips incidence was recorded as average counts per plot through regular expert field scouting.

B. Multispectral data acquisition and analysis

Multispectral data were acquired using a MicaSense RedEdge-P sensor [23] mounted on a quadcopter. This sensor captures Blue, Green, Red, Red Edge, and Near-Infrared bands, complemented by a high-resolution panchromatic band. To ensure optimal solar illumination and minimize shadows, autonomous missions were executed via *Mission Planner* between 10:00 AM and 1:00 PM at an altitude of 30 m and a speed of 5 m/s. This configuration yielded a ground sampling distance of approximately 2.0 cm/pixel. As illustrated in the workflow in Fig. 2, photogrammetric processing was performed using Pix4Dmapper [24] to generate geometrically aligned and radiometrically calibrated orthomosaics for all spectral bands. To isolate pure canopy pixels and minimize soil-induced spectral contamination, a dynamic vegetation mask was manually created and co-registered across all bands. The preprocessing module then extracted the mean values for the vegetation indices (VIs) detailed in Table I. These indices were selected for their theoretical ability to capture distinct physiological traits, including canopy biomass, chlorophyll concentration, and photosynthetic activity.

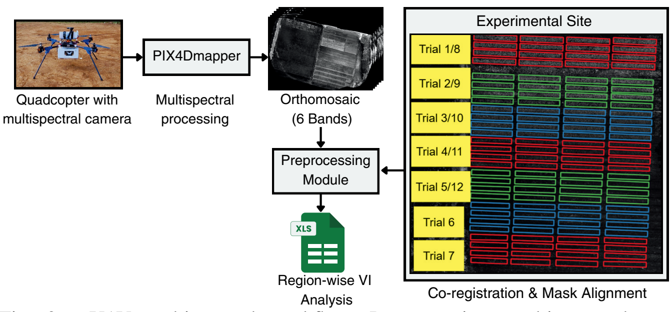

Fig. 2. UAV multispectral workflow: Preprocessing, multitemporal co-registration, and region-wise VI time-series analysis.

1) Exploratory Data Analysis (EDA): A rigorous EDA was conducted through univariate distribution analysis and outlier detection, followed by Spearman rank correlations and scatter plot visualizations to investigate the relationships between VIs and ground-truth stressors. The initial hypothesis assumed a conventional inverse relationship: as disease severity increases, health-associated VI values decrease. However, as shown in the 'Correlation (Normal)' heatmap (Fig. 3), preliminary analysis across the growth cycle revealed a paradoxical, statistically significant positive correlation between VIs (e.g., NDVI, GNDVI) and fungal severity, notably stemphylium blight.
This counter-intuitive finding indicates that the direct relationship was being obscured by a powerful confounding variable: plant biomass. The underlying mechanism is likely twofold: first, inherently healthier, more vigorous plants generate higher biomass, which yields higher VI values regardless of infection; and second, the resulting dense canopy establishes a humid microclimate that facilitates fungal pathogen proliferation. Consequently, a spurious correlation emerges where high VI values, driven by biomass, are falsely associated with high disease severity. To validate this hypothesis, the dataset was stratified into three distinct phenological stages based on days after transplanting (DAT): vegetative (< 50 DAT), bulb initiation (51–70 DAT), and bulb development (> 70 DAT). The analysis confirmed that the positive correlation was strongest during the bulb initiation stage, reinforcing the hypothesis that high-biomass plants were most susceptible to disease.

2) Feature Engineering: To address the biomass paradox and isolate the true physiological stress signal, two novel sets of features were engineered:

- **Temporal Features:** To capture plant health dynamics, delta (Δ, rate of change between consecutive observations) and lagged ($\mathcal{L}$, the value from the previous observation) features were computed for each plot's time-series. These temporal features provide critical historical context, enabling the model to learn from the growth trajectory rather than static states.
- **Biomass-normalized Features:** To decouple physiological health from biomass signals, we derived ratio ($\mathcal{R} = \frac{VI}{NDVI}$) and difference ($\mathcal{D} = VI - NDVI$) features by normalizing health-sensitive indices (e.g., NDRE) against NDVI, a canopy-vigor proxy linked to vegetation fraction, LAI, and biomass [25, 26]. By utilizing $\mathcal{R}$ and $\mathcal{D}$ features, this 'health per unit of biomass' metric mitigates confounding influence of plant size, enabling the model to distinguish biomass-driven spectral intensity from genuine physiological decline.

The efficacy of these transformations is confirmed by the 'Correlation (Delta)' heatmap (Fig. 3). Unlike the normal correlations, the delta features exhibit the expected negative correlations with disease severity. This shift confirms that the engineered features successfully resolved the biomass paradox. Consequently, the final multispectral feature vector comprises mean VIs, temporal features, and biomass-normalized features,

TABLE I
SPECTRAL AND VEGETATION INDICES USED IN THIS STUDY

Index	Formula
Normalized Difference Vegetation Index (NDVI [10])	$(NIR - RED)/(NIR + RED)$
Green Normalized Difference Vegetation Index (GNDVI [11])	$(NIR - GREEN)/(NIR + GREEN)$
Soil-Adjusted Vegetation Index (SAVI [12])	$((NIR - RED)/(NIR + RED + L)) * (1 + L)$
Enhanced Vegetation Index 2 (EVI2 [13])	$2.5 \times (NIR - RED)/(NIR + 2.4 \times RED + 1)$
Leaf area index (LAI [14])	$(3.618 \times 2.5 \times (NIR - RED))/(NIR + 6 \times RED - 7.5 \times BLUE + 1) - 0.118$
Normalized Difference Red Edge (NDRE [15])	$(NIR - REDEDGE)/(NIR + REDEDGE)$
Red Edge Chlorophyll Index (CI-RE [16])	$(NIR/REDEDGE) - 1$
Visible Atmospherically Resistant Index (VARI [17])	$(GREEN - RED)/(GREEN + RED - BLUE)$
Normalized Green Red Difference Index (NGRDI [18])	$(GREEN - RED)/(GREEN + RED)$
Difference Vegetation Index (DVI [19])	$NIR - RED$
Simple Ratio (SR [20])	NIR/RED
Green Stress Ratio (GSR †)	$(GREEN)/(NIR + RED)$
Kawashima Index (IKAW [21])	$(RED - BLUE)/(RED + BLUE)$
Plant Senescence Reflectance Index (PSRI [22])	$(RED - BLUE)/REDEDGE$

† GSR highlights stress-driven reductions in green reflectance relative to structural (NIR) and absorptive (RED) components. It showed the strongest correlation with stress-related delta features for stemphylium blight, anthracnose, purple blotch, and thrips.

which are further complemented by engineered meteorological features.

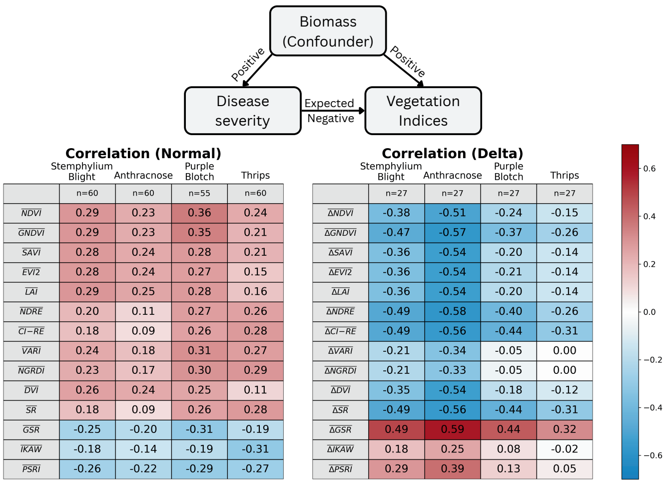

Fig. 3. Biomass confounds relationships between disease severity and vegetation indices: conventional correlations largely reflect canopy vigor, whereas delta features suppress biomass effects and better capture physiological stress. Here, n denotes the number of observation days (1 day = 1 data point).

C. Weather data acquisition and analysis

Continuous environmental monitoring was achieved using a solar-powered indigenous IoT weather station (SAMBHAV™) deployed within the DOGR fields (Fig. 4), recording soil and atmospheric parameters at 15-minute intervals for cloud-based analysis [27]. For this study, temperature (T), relative humidity (RH), and rainfall were used to characterize environmental stress drivers. During the experiment, temperature ranged from 22–31 °C and relative humidity from 35–85%, indicating substantial variability. These meteorological variables are fundamental to pest population dynamics, as elevated temperatures can accelerate pest life cycles while fluctuations in humidity and rainfall impact pathogen survival and dispersal [28]. To capture these shifts more effectively than static daily averages, delta features for temperature (ΔT) and relative humidity (ΔRH) were engineered. By partitioning diurnal data into five blocks between 4:00 AM and 4:00 PM, we calculated the delta features as the difference between the early

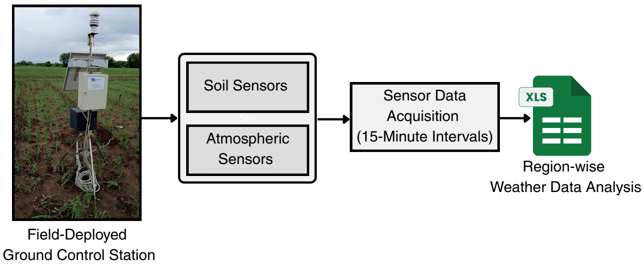

Fig. 4. Operational workflow of the SAMBHAV™ weather station.

morning (4:00–8:00 AM) and midday (10:00 AM–2:00 PM) averages. This methodology captures the magnitude of daily environmental transitions, which are often more indicative of stress than mean values. For rainfall, daily totals (R_t) and 7-day rolling averages ($\bar{R}_{prev7}$) were calculated to assess lagged moisture and precipitation-driven stress on crop health. Correlation between these environmental parameters and biotic stress incidence is summarized in Fig. 5.

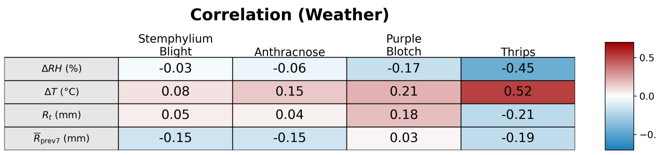

Fig. 5. Atmospheric measurements correlation

D. Two-Stage Hurdle Modeling for Crop Stress Estimation

Using the combined multispectral and meteorological feature set, we implemented a unified machine learning pipeline using a two-stage hurdle strategy to account for zero-inflated, right-skewed response variables. In *Stage 1 (Presence)*, a binary classifier estimates the probability of stress occurrence $P(\text{presence})$, where the target is $y > 0$. *Stage 2 (Severity)* then models stress intensity using only non-zero observations, with targets log-transformed ($f(x) = \log(1 + x)$) to stabilize variance. The final estimate ($\hat{y}$) combines both stages:

$$\hat{y} = P(\text{presence}) \times (\exp(\hat{s}) - 1) \tag{1}$$

where $\hat{s}$ is the predicted log-severity. To prevent data leakage from repeated temporal measures, group-aware cross-validation ensured samples from the same experimental trial were never shared between training and validation folds.

Three paired configurations are evaluated: *tree-based* (Random Forest classifier and regressor), *non-linear* (SVM and SVR with RBF Kernel), and *linear* (Logistic Regression and OLS).

III. Results

Target-specific features were engineered to capture unique stress signatures. Beyond vegetation indices, we computed temporal and structural transformations, including first and second derivatives (Δ, Δ^2), lagged states ($\mathcal{L}$), and biomass-normalized ratios ($\mathcal{R}$) and differences ($\mathcal{D}$), to track acute dynamics and chronic vigor deviations. Feature relevance was determined via trial-independent correlation analysis, prioritizing robust features with high mean correlation and low inter-trial variability. Feature selection was conducted separately for each hurdle stage. Presence (class.) models utilized trials with both stress presence and absence to avoid degenerate associations, while severity (regr.) models were optimized using only non-zero observations. Although multispectral features were target and stage specific, all four weather variables were consistently included in every model to account for environmental drivers. Final subsets are summarized in Table II.

TABLE II
Selected Input Features Grouped by Transformation Symbol

Target	**Model**	**Spectral Features (Grouped by Symbol)**
Stemphylium blight	Class.	Δ(PSRI); Δ^2(GSR, CI-RE, DVI); $\mathcal{D}$(CI-RE)
	Regr.	μ(GNDVI); Δ(CI-RE, SR, NDRE, EVI2); $\mathcal{R}$(NGRDI, VARI); $\mathcal{D}$(EVI2, SAVI)
Anthracnose	Class.	Δ(PSRI, DVI, NDVI, NDRE, GNDVI); Δ^2(NDRE, GNDVI, CI-RE, GSR, IKAW, NGRDI, SAVI)
	Regr.	μ(GNDVI, NDVI, NGRDI, VARI, SR, CI-RE, NDRE, SAVI, EVI2, LAI); Δ(IKAW); Δ^2(DVI); $\mathcal{L}$(GNDVI, NDVI, NGRDI, VARI)
Purple blotch	Class.	Δ(SAVI, NGRDI); Δ^2(GSR, PSRI, IKAW, NDRE, CI-RE)
	Regr.	μ(EVI2, SAVI, NDVI); Δ(LAI); Δ^2(LAI)
Thrips	Class.	$\mathcal{R}, \mathcal{D}, \mathcal{L}$ (GSR, GNDVI, SAVI)
	Regr.	$\mu, \Delta, \Delta^2, \mathcal{R}, \mathcal{D}$ (GNDVI, LAI, SAVI, GSR, PSRI, IKAW)

Common Features: All models include Days After Transplanting (DAT) and meteorological variables ($\Delta RH, \Delta T, R_t, \bar{R}_{prev7}$).
Transformations: Temporal mean (μ), first/second-order derivatives (Δ, Δ^2), lagged state ($\mathcal{L}$), and biomass-normalized ratio/difference features ($\mathcal{R}, \mathcal{D}$).

Model performance was evaluated across both hurdle stages using standard metrics: F1-score and Area Under the Receiver Operating Characteristic Curve (AUC) for classification (presence), and RMSE, MAE, and R^2 for regression (severity). Classification metrics assess stress detection, while regression metrics quantify precision and variance in severity estimation. Results are summarized in Table III.

TABLE III
Performance of Hurdle Models for Diseases and Pests

Disease / Pest	**Hurdle Model**	**F1@0.5**	**AUC**	**RMSE**	**MAE**	$\mathbf{R^2}$
Stemphylium blight	Random Forest	0.80	0.85	12.60	6.91	0.35
	SVM/R	0.73	0.77	14.43	8.42	0.15
	Linear	0.72	0.92	14.61	8.53	0.13
Anthracnose	Random Forest	0.80	0.78	15.23	23.27	0.12
	SVM/R	0.74	0.76	17.43	24.59	0.01
	Linear	0.73	0.72	13.76	22.28	0.19
Purple blotch	Random Forest	0.82	0.93	7.95	4.06	0.17
	SVM/R	0.63	0.85	9.41	5.53	−0.17
	Linear	0.65	0.82	23.41	11.41	−6.22
Thrips	Random Forest	0.78	0.80	23.27	15.23	0.12
	SVM/R	0.76	0.74	24.59	17.43	0.01
	Linear	0.72	0.73	22.28	13.76	0.19

The Random Forest (RF) hurdle model delivered the most consistent performance, achieving its best results for Purple blotch (AUC = 0.9312, F1 = 0.8169) and for Stemphylium blight regression (highest R^2 = 0.3545, lowest MAE = 6.9129), but performed weaker for Thrips (R^2 = 0.1179, F1 = 0.7754), where a Linear model showed better variance capture (R^2 = 0.1908); SVM/R consistently underperformed, including negative R^2 for Purple blotch. Severity estimation in agricultural time-series remains challenging due to environmental variability, annotation noise, and limited ground truth; therefore, this work prioritizes detection over regression, and the reported values R^2 should be considered preliminary. Despite modest regression performance, the proposed temporal delta and normalized features improve classification, as reflected in strong F1-scores; this contrast arises because R^2 measures variance in continuous labels, whereas F1 evaluates binary decisions less sensitive to label noise. The differences between MAE and RMSE reflect the error distribution, with RMSE penalizing larger deviations more strongly, while MAE remains relatively stable, which is typical of noisy real-world regression tasks.

IV. Discussion

This study integrated aerial multispectral imagery with weather data to estimate diseases and pest incidence in Bhima onions under co-occurring field conditions. We evaluated fourteen vegetation indices and four weather parameters, incorporating temporal and biomass transformations to capture stress dynamics. Notably, a derived *Green Stress Ratio* vegetation index exhibited the highest correlation across all stressors. A two-stage hurdle model was implemented to automate classification and severity regression for Stemphylium blight, anthracnose, purple blotch, and thrips.

By automating the detection and severity estimation of major stressors, this framework supports precision onion cultivation and reduces reliance on labor-intensive manual inspections. These outputs enable targeted agronomic advisories, such as the selective application of fungicides and pesticides, while providing a scalable foundation for future yield prediction in the Bhima onion variety. Although the study successfully demonstrated effectiveness over a single season (August 2023–March 2024), future work will focus on validating the framework across at least four consecutive years to ensure robustness against inter-annual climatic and phenological variability. Furthermore, transitioning from controlled plots to heterogeneous farms is essential to verify applicability under operational conditions.

References

[1] Press Information Bureau, Government of India, "2.60 lakh tons of onion exported in 2024-25, till 31st july, 2024; centre procures 4.68 lakh tons for price stabilisation buffer," August 7 2024, accessed: Jan. 2026. [Online]. Available: https://www.pib.gov.in/PressReleasePage.aspx?PRID=2042765&reg=3&lang=2

[2] A. Raj, M. Dawale, S. Wayal, K. Khandagale, I. Bhangare, S. Banerjee, A. Gajarushi, R. Velmurugan, M. S. Baghini, and S. Gawande, "Yolo-odd: an improved yolov8s model for onion foliar disease detection," *Frontiers in Plant Science*, vol. 16, p. 1551794, 2025.

[3] H. M. Abdullah, N. T. Mohana, B. M. Khan, S. M. Ahmed, M. Hossain, K. S. Islam, M. H. Redoy, J. Ferdush, M. Bhuiyan, M. M. Hossain *et al.*, "Present and future scopes and challenges of plant pest and disease (p&d) monitoring: Remote sensing, image processing, and artificial intelligence perspectives," *Remote Sensing Applications: Society and Environment*, vol. 32, p. 100996, 2023.

[4] R. Alberto, J. Rivera, A. Biagtan, and M. Isip, "Extraction of onion fields infected by anthracnose-twister disease in selected municipalities of nueva ecija using uav imageries," *Spatial Information Research*, vol. 28, no. 3, pp. 383–389, 2020.

[5] M. R. McDonald, C. S. Tayviah, and B. D. Gossen, "Human vs. machine, the eyes have it. assessment of stemphylium leaf blight on onion using aerial photographs from an nir camera," *Remote Sensing*, vol. 14, no. 2, p. 293, 2022.

[6] S. Rizwana, K. Giridhar, B. T. Priya, and K. U. Krishna, "Impact of different weather parameters on thrips population (thrips parvispinus karny) in chilli," *International Journal of Research in Agronomy*, vol. 7, no. 12, pp. 95–98, 2024.

[7] D. Mandal, R. Pal, and I. Kar, "Effect of weather parameters on the progression and development of purple blotch of onion," *Journal of Agrometeorology*, vol. 24, no. 3, pp. 325–327, 2022.

[8] Q. Zheng, H. Ye, W. Huang, Y. Dong, H. Jiang, C. Wang, D. Li, L. Wang, and S. Chen, "Integrating spectral information and meteorological data to monitor wheat yellow rust at a regional scale: A case study," *Remote Sensing*, vol. 13, no. 2, p. 278, 2021.

[9] C. Ruan, Y. Dong, W. Huang, L. Huang, H. Ye, H. Ma, A. Guo, and R. Sun, "Integrating remote sensing and meteorological data to predict wheat stripe rust," *Remote sensing*, vol. 14, no. 5, p. 1221, 2022.

[10] A. Karnieli, N. Agam, R. T. Pinker, M. Anderson, M. L. Imhoff, G. G. Gutman, N. Panov, and A. Goldberg, "Use of ndvi and land surface temperature for drought assessment: Merits and limitations," *Journal of climate*, vol. 23, no. 3, pp. 618–633, 2010.

[11] A. A. Gitelson, Y. J. Kaufman, and M. N. Merzlyak, "Use of a green channel in remote sensing of global vegetation from eos-modis," *Remote sensing of Environment*, vol. 58, no. 3, pp. 289–298, 1996.

[12] A. R. Huete, "A soil-adjusted vegetation index (savi)," *Remote sensing of environment*, vol. 25, no. 3, pp. 295–309, 1988.

[13] Z. Jiang, A. R. Huete, K. Didan, and T. Miura, "Development of a two-band enhanced vegetation index without a blue band," *Remote sensing of Environment*, vol. 112, no. 10, pp. 3833–3845, 2008.

[14] L. Andalibi, A. Ghorbani, M. Moameri, Z. Hazbavi, A. Nothdurft, R. Jafari, and F. Dadjou, "Leaf area index variations in ecoregions of ardabil province, iran," *Remote Sensing*, vol. 13, no. 15, p. 2879, 2021.

[15] C. N. Thompson, W. Guo, B. Sharma, and G. L. Ritchie, "Using normalized difference red edge index to assess maturity in cotton," *Crop Science*, vol. 59, no. 5, pp. 2167–2177, 2019.

[16] A. A. Gitelson, A. Viña, V. Ciganda, D. C. Rundquist, and T. J. Arkebauer, "Remote estimation of canopy chlorophyll content in crops," *Geophysical research letters*, vol. 32, no. 8, 2005.

[17] A. A. Gitelson, Y. J. Kaufman, R. Stark, and D. Rundquist, "Novel algorithms for remote estimation of vegetation fraction," *Remote sensing of Environment*, vol. 80, no. 1, pp. 76–87, 2002.

[18] C. J. Tucker, "Red and photographic infrared linear combinations for monitoring vegetation," *Remote sensing of Environment*, vol. 8, no. 2, pp. 127–150, 1979.

[19] A. J. Richardson and C. Weigand, "Distinguishing vegetation from soil background information," *Photogrammetric engineering and remote sensing*, vol. 43, no. 12, 1977.

[20] C. F. Jordan, "Derivation of leaf-area index from quality of light on the forest floor," *Ecology*, vol. 50, no. 4, pp. 663–666, 1969.

[21] S. Kawashima and M. Nakatani, "An algorithm for estimating chlorophyll content in leaves using a video camera," *Annals of Botany*, vol. 81, no. 1, pp. 49–54, 1998.

[22] M. N. Merzlyak, A. A. Gitelson, O. B. Chivkunova, and V. Y. Rakitin, "Non-destructive optical detection of pigment changes during leaf senescence and fruit ripening," *Physiologia plantarum*, vol. 106, no. 1, pp. 135–141, 1999.

[23] AgEagle Aerial Systems Inc., "Micasense rededge-p: Multispectral and panchromatic imaging system," Product Brochure, 2022, online. [Online]. Available: https://ageagle.com/wp-content/uploads/2022/08/AgEagle-RedEdge-P-Brochure-EN.pdf

[24] Pix4D SA, *Pix4Dmapper: Photogrammetry Software for Mapping and 3D Modeling*, Pix4D SA, Lausanne, Switzerland, 2022. [Online]. Available: https://www.pix4d.com/product/pix4dmapper

[25] A. A. Gitelson, "Wide dynamic range vegetation index

for remote quantification of biophysical characteristics of vegetation," *Journal of plant physiology*, vol. 161, no. 2, pp. 165–173, 2004.

[26] P. J. Zarco-Tejada, J. R. Miller, T. L. Noland, G. H. Mohammed, and P. H. Sampson, "Scaling-up and model inversion methods with narrowband optical indices for chlorophyll content estimation in closed forest canopies with hyperspectral data," *IEEE transactions on geoscience and remote sensing*, vol. 39, no. 7, pp. 1491–1507, 2002.

[27] P. Banerjee, P. Behera, S. Bansode, A. Gajarushi, L. Vachhani, M. S. Baghini, and A. Thangasamy, "Performance analysis of soil sensors: Accuracy, variability, and repeatability," in *2025 IEEE Applied Sensing Conference (APSCON)*. IEEE, 2025, pp. 311–314.

[28] R. Shafique, S. H. Khan, J. Ryu, and S. W. Lee, "Weather-driven predictive models for jassid and thrips infestation in cotton crop," *Sustainability*, vol. 17, no. 7, p. 2803, 2025.